
CLIPArTT: LIGHT-WEIGHT ADAPTATION OF CLIP TO NEW DOMAINS AT TEST TIME

A PREPRINT

Gustavo A. Vargas Hakim* David Osowiechi* Mehrdad Noori Milad Cheraghalikhani Ali Bahri

Moslem Yazdanpanah

Ismail Ben Ayed

Christian Desrosiers

LIVIA, ÉTS Montréal, Canada
International Laboratory on Learning Systems (ILLS),
McGILL - ETS - MILA - CNRS - Université Paris-Saclay - CentraleSupélec, Canada
gustavo-adolfo.vargas-hakim.1@ens.etsmtl.ca, david.osowiechi.1@ens.etsmtl.ca

ABSTRACT

Pre-trained vision-language models (VLMs), exemplified by CLIP, demonstrate remarkable adaptability across zero-shot classification tasks without additional training. However, their performance diminishes in the presence of domain shifts. In this study, we introduce CLIP Adaptation duRing Test-Time (CLIPArTT), a fully test-time adaptation (TTA) approach for CLIP, which involves automatic text prompts construction during inference for their use as text supervision. Our method employs a unique, minimally invasive text prompt tuning process, wherein multiple predicted classes are aggregated into a single new text prompt, used as *pseudo label* to reclassify inputs in a transductive manner. Additionally, we pioneer the standardization of TTA benchmarks (e.g., TENT) in the realm of VLMs. Our findings demonstrate that, without requiring additional transformations nor new trainable modules, CLIPArTT enhances performance dynamically across non-corrupted datasets such as CIFAR-10, corrupted datasets like CIFAR-10-C and CIFAR-10.1, alongside synthetic datasets such as VisDA-C. This research underscores the potential for improving VLMs' adaptability through novel test-time strategies, offering insights for robust performance across varied datasets and environments. The code can be found at: <https://github.com/dosowiechi/CLIPArTT.git>

1 Introduction

Combining vision and language modalities for learning, namely a Vision Language model (VLM), has demonstrated an outstanding performance in different vision tasks Radford et al. [2021], Jia et al. [2021], Kirillov et al. [2023]. Remarkably, these models are surprisingly effective at zero-shot generalization, where a new task can be outside the original scope of the training set, without any additional supervision to fine tune the model. Models such as CLIP Radford et al. [2021] have then been employed in fields as diverse as video recognition Lin et al. [2022], audio Guzhov et al. [2022], and medical imaging Liu et al. [2023]. These advancements point these methods to become critical in future machine learning research and applications.

As in other more traditional deep architectures (e.g., CNNs), CLIP is prone to performance degradation on domains to which it was not originally exposed. Recent research trends suggest that domain adaptation mechanisms can play an important role in deploying CLIP Lai et al. [2023], Shu et al. [2022]. The challenge, however, is to adapt the model to new domains in real-time and as fast as possible, to maintain its attractive zero-shot capabilities without the need of retraining.

In this paper, CLIP is contextualized in the setting of Test-Time Adaptation, a challenging yet practical scenario of domain adaptation. In realistic scenarios, a model needs to adapt to new data *on-the-fly* to cope with unknown

*Equal contribution

distribution shifts, and without using any class supervision. Although an experimental boilerplate was standardized in recent years, CLIP has not been integrated to it yet. Additionally, we introduce a powerful adaptation technique that achieves *state-of-the-art* performance without a significant computational overhead. Comprehensive studies are performed on three datasets containing different types of domain shifts on several levels of severity, resulting in a total of 155 evaluation scenarios. Our main contributions can then be summarized as follows:

- We propose a light-weight Test-Time Adaptation method for CLIP, called CLIPArTT, that adapts this VLM to new domains without a considerable computation overhead.
- We introduce a new benchmark for Test-Time Adaptation on Vision-Language Models by implementing representative baselines, such as TENT.
- Through comprehensive experiments, we subject our CLIPArTT methodology to diverse and challenging Test-Time Adaptation scenarios, each characterized by distinct types of domain shifts. The outcomes of these experiments highlight the performance of our approach when compared against other methodologies addressing similar challenges.

The rest of the paper is organized in the following sections. Section 2 compiles significant related work to contextualize our method. Section 3 introduces CLIPArTT and explains its functionality. Section 4 details the experimental setting, with results exposed in Section 5. Section 6 concludes with a summary of contributions and potential future work.

2 Related work

Test-Time Adaptation. TTA is a particular setting of Domain Adaptation, encompassing two main characteristics: (a) adapting a model to a target domain, with inputs coming as unlabeled data streams (i.e., batches), without (b) any access to the source domain samples. The former challenge complicates accurately estimating the target domain’s distribution, while the latter impedes solving the problem by directly comparing domains’ characteristics such as statistics. Despite the challenging nature of the problem, the field has gained important momentum in recent years, providing insights on the possibilities and limitations of adapting pre-trained models.

An important branch of TTA methods targets batch normalization layers for adaptation, as they can keep key information from the source domain. As the simplest approach, PTBN Nado et al. [2021] addresses the problem by simply recomputing the batch statistics at test-time. TENT Wang et al. [2021] goes further by using entropy minimization on the model’s predictions as feedback, and optimizes the affine parameters in batch normalization layers after one iteration. Entropy minimization has since been a recurrent alternative to update models to target domains without label supervision Goyal et al. [2022], Zhang et al. [2022], Lin et al. [2023], Lee et al. [2023] by increasing the model’s confidence. These approaches, however, rely on image augmentations or large batches to be effective. More recently, methods such as Text-Prompt Tuning (TPT) Shu et al. [2022] have introduced entropy minimization to adapt CLIP, while focusing on learning an adapter for the text prompts. However, this method heavily relies on input augmentations, making it more costly to train. Our method also fine-tunes normalization layers to have a minimal impact on the model’s knowledge and utilizes the confidence of the predictions to improve the text supervision. Moreover, we do not employ any augmentations on the inputs.

Pseudo-labels have also played an important role in previous TTA research. SHOT Liang et al. [2020] employs them with cross-entropy to regularize mutual information between inputs and predictions. The entire feature encoder is optimized in this case. CoTTA Wang et al. [2022] makes use of pseudo-labels in the context of a student-teacher model, where one model processes the original input and the other processes augmented versions of that input. A consistency loss is used to compare both models’ outputs. PAD Wu et al. [2021] improves the quality of pseudo-labels by also augmenting inputs and using voting on the models’ predictions. Instead of simple class pseudo-labels, CLIPArTT improves the text supervision to broaden the likelihood of accurately predicting the right class.

Some other methods utilize less conventional approaches for TTA. LAME Boudiaf et al. [2022] refines the classifier’s predictions in a transductive manner using the similarity between features through the Laplacian. A family of test-time training (TTT) methods have also gained popularity Sun et al. [2020], Liu et al. [2021], Osowiechi et al. [2023], Gandelsman et al. [2022], Vargas Hakim et al. [2023], Osowiechi et al. [2024], where a sub-branch is trained alongside the main network in an unsupervised way, which is later used to update the model. These methods require training the model from scratch on the source domain. As LAME, our method is related to the concept of Laplacian regularization, however we exploit this concept very differently. Whereas LAME employs it to refine predictions in a traditional transductive inference approach where the model is kept *as is*, our method exploits in a test-time adaptation loss enforcing the consistency between embeddings of related batch samples. Contrary to TTT methods, we do not train the model from scratch with any additional branch.

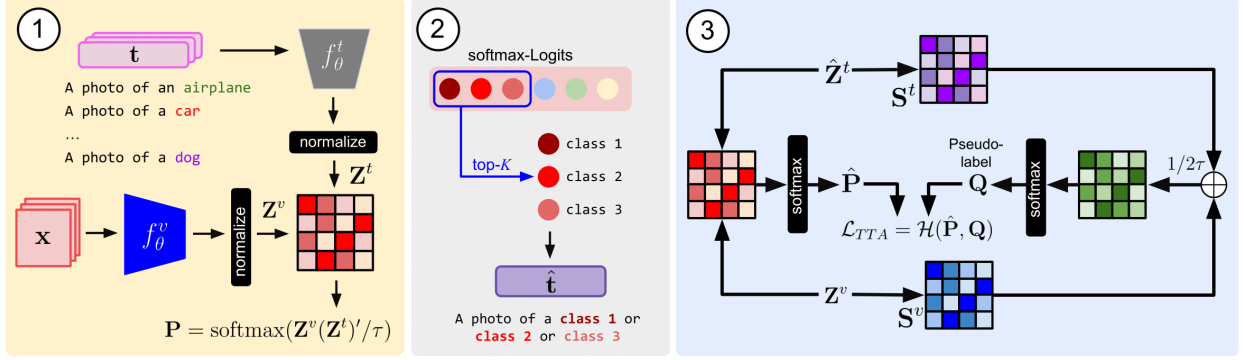


Figure 1: CLIPArTT pipeline overview: 1) Computing predictions from Image-Text Similarity, 2) generating a new text prompt by filtering the top- K class predictions, 3) employing the new prompt to obtain image-to-image and text-to-text similarity scores, used to build a pseudo-label for cross-entropy.

Conformal Learning. CLIPArTT is also related to the field of conformal learning, where intervals of confidence for new predictions are derived from previous experience Shafer and Vovk [2008]. In a conformal prediction, a given level of certainty is assigned to a set $\mathcal{C} = \{c_1, \dots, c_K\}$ with the K most plausible classes that an input can belong to Angelopoulos and Bates [2021]. We draw inspiration from this concept and build a conformal set of class predictions that can help adapting CLIP towards an accurate top-1 prediction. Our technique, however, stands out by not relying on image transformations such as in Shu et al. [2022], Lai et al. [2023] to filter out predictions.

3 Methodology

We start by presenting the vanilla CLIP model for classification and explain how it can be extended to test-time adaptation using entropy minimization. Building on the limitations of this approach, we then introduce our CLIPArTT method that leverages class uncertainty and the relationship between samples in a batch.

3.1 CLIP-based classification

Contrastive Language-Image Pre-training (CLIP) Radford et al. [2021] consists of a visual encoder $f_\theta^v(\cdot)$, mapping an image \mathbf{x} to visual features $\mathbf{z}^v \in \mathbb{R}^D$, and a text encoder $f_\theta^t(\cdot)$ transforming text prompts \mathbf{t} to text features $\mathbf{z}^t \in \mathbb{R}^D$. The visual and text encoders are trained jointly with a contrastive loss so that the feature embeddings of training images and their corresponding text prompt are close to each other, while those of different training examples are pushed apart.

In a classification task with K fixed classes, CLIP can be used to perform inference by encoding a pre-defined text prompt for each class, for example $\mathbf{t}_k = \text{"a photo of a \{class } k\}"$. For a new image \mathbf{x}_i , the probability of belonging to class k is then estimated based on cosine similarity,

$$p_{ik} = \frac{\exp(\cos(\mathbf{z}_i^v, \mathbf{z}_k^t)/\tau)}{\sum_j \exp(\cos(\mathbf{z}_i^v, \mathbf{z}_j^t)/\tau)}, \quad \cos(\mathbf{z}, \mathbf{z}') = \frac{\mathbf{z}^\top \mathbf{z}'}{\|\mathbf{z}\|_2 \cdot \|\mathbf{z}'\|_2}, \quad (1)$$

where τ is a suitable softmax temperature.

The model in Eq. (1) can be used for test-time adaptation in various ways, the simplest one being entropy minimization as in TENT. This approach, which relies on the principle that the decision boundary lies in a low-density region of space giving rise to a low prediction entropy, adapts the model parameters by minimizing entropy on a test batch of size B :

$$\mathcal{L}_{\text{TENT}}(\theta) = -\frac{1}{B} \sum_{i=1}^B \sum_{k=1}^K p_{ik} \log p_{ik} \quad (2)$$

However, this approach as well as similar ones based on pseudo-labels Liang et al. [2020], Wang et al. [2022], Wu et al. [2021] suffer from two important limitations. First, due to domain shifts, the model’s prediction may be unreliable (e.g., giving the highest probability to the wrong class) and techniques such as entropy minimization or standard

	CIFAR10		CIFAR100	
	Top-1	Top-3	Top-1	Top-3
Original	88.74	97.79	61.68	80.92
C-Average	59.22	82.43	29.43	46.61

Table 1: Accuracy (%) on CIFAR-10/100 and CIFAR-10/100-C datasets with Level 5 corruption for the top-1 or the top-3 predicted classes.

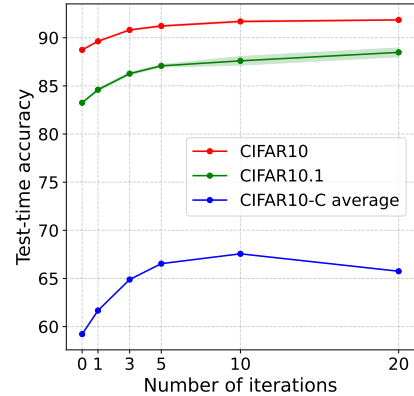


Figure 2: Evolution of the accuracy after several iterations of adaptation at test-time for TENT.

pseudo-label will only reinforce these errors during adaptation. Secondly, they assume that samples in a test batch are independent and do not directly leverage their semantic relationships.

3.2 Our CLIPArTT method

The proposed CLIPArTT method, illustrated in Figure 1, addresses the above-mentioned limitations using two key insights. The first insight, inspired by conformal learning, is that the correct class is often among the ones with the highest probabilities, although the model’s most confident prediction may not be always correct. This claim is supported by the results in Table 13 (*Original*), showing that the correct class is within the top-3 predictions 97.79% of the times for CIFAR10 (versus 88.74% within the top-1), and 80.92% of the times for CIFAR100 (versus 61.68% within the top-1). A way to include information about multiple classes could, therefore, help adapting the model at test time. The second insight is that the similarity between the batch samples could be evaluated based on their visual and/or text embeddings. As we will show below, such similarities could be exploited in a strategy related to graph-Laplacian regularization.

Instance-specific multi-class prompt Inspired by our first insight, we devise a novel technique to generate instance-specific prompts from the top- k predictions, with $1 \leq k \ll K$. Specifically, for an image \mathbf{x}_i , we estimate the CLIP-based class probabilities using Eq. (1) and then generate a new text prompt as $\hat{\mathbf{t}}_i = \text{a photo of a } \{\text{class } i_1\} \text{ or } \dots \text{ or } \{\text{class } i_k\}$, where $\{\text{class } i_j\}$ is the name of the class with j -th highest probability.

Transductive TTA Next, we design a test-time adaptation loss that accounts for semantic relationships between batch samples. Let $\mathbf{Z}^v \in \mathbb{R}^{B \times D}$ and $\hat{\mathbf{Z}}^t \in \mathbb{R}^{B \times D}$ denote the *normalized* visual and instance-specific text embeddings of the samples within the test batch, respectively. We compute an image-to-image similarity matrix, $\mathbf{S}^v = \mathbf{Z}^v (\mathbf{Z}^v)^\top \in [-1, 1]^{B \times B}$, and a text-to-text similarity matrix, $\mathbf{S}^t = \hat{\mathbf{Z}}^t (\hat{\mathbf{Z}}^t)^\top \in [-1, 1]^{B \times B}$. The former measures the affinity between each pair of samples within the batch in terms of their visual characteristics (shapes, textures, etc.). The latter captures common (or related) classes in the top- k predictions of two samples, since it is computed using the instance-specific multi-class prompts.

We deploy these two pairwise similarity matrices to compute pseudo-labels as follows:

$$\mathbf{Q} = \text{softmax}((\mathbf{S}^v + \mathbf{S}^t)/2\tau) \in [0, 1]^{B \times B} \quad (3)$$

where the softmax operation is applied column-wise and the temperature $\tau = 0.01$ in all our experiments.

Let $\hat{\mathbf{P}}$ denotes the zero-shot prediction matrix using our instance-specific multi-class text prompts:

$$\hat{\mathbf{P}} = \text{softmax}(\mathbf{Z}^v (\hat{\mathbf{Z}}^t)^\top / \tau), \quad \hat{p}_{ij} = \frac{\exp(\cos(\mathbf{z}_i^v, \hat{\mathbf{z}}_j^t) / \tau)}{\sum_k \exp(\cos(\mathbf{z}_i^v, \hat{\mathbf{z}}_k^t) / \tau)} \quad (4)$$

This matrix, along with the pairwise pseudo-labels we introduced in Eq. (3), yield our final TTA loss based on the cross-entropy:

$$\mathcal{L}_{\text{TTA}}(\theta) = -\frac{1}{B} \sum_{i=1}^B \sum_{j=1}^B q_{ij} \log \hat{p}_{ij}. \quad (5)$$

Unlike recent approaches Shu et al. [2022], which adapt the CLIP model by learning a text prompt, we instead update the normalization-layer parameters of the *visual* encoder, which yields a light-weight, computationally efficient TTA method.

3.3 Link to graph-Laplacian regularization

An important element of our TTA method is that it exploits the similarities between pairs of samples within the batch, in terms of the visual features and text prompts representing the top- k classes. In this section, we draw a connection between the proposed method and graph-Laplacian regularization, well-known in the context semi-supervised learning techniques Chapelle et al. [2006] and label propagation Iscen et al. [2019]. In our case, the Laplacian regularizer is computed over a set of B nodes with predictions $\mathbf{Z} \in \mathbb{R}^{B \times D}$ as

$$\mathcal{L}_{\text{reg}}(\mathbf{Z}) = \text{trace}(\mathbf{Z}^\top \mathbf{L}_W \mathbf{Z}) = \sum_{i,j} w_{ij} \|\mathbf{z}_i - \mathbf{z}_j\|_2^2, \quad (6)$$

where $\mathbf{L}_W \in \mathbb{R}^{B \times B}$ is the Laplacian matrix defined from edge weight matrix \mathbf{W} as follows:

$$[\mathbf{L}_W]_{ij} = \begin{cases} d_{ii} = \sum_j w_{ij}, & \text{if } i = j \\ -w_{ij} & \text{else.} \end{cases} \quad (7)$$

This connection is made in the following proposition.

Proposition 1. *The TTA loss in Eq. (5) can be expressed as a Laplacian regularization over a bipartite graph with one set of nodes for image embeddings and another for text embeddings.*

Proof. Expanding the softmax in Eq. (5), we get

$$\mathcal{L}_{\text{TTA}} = -\frac{1}{B} \sum_{i=1}^B \sum_{j=1}^B q_{ij} \log \frac{\exp((\mathbf{z}_i^v)^\top \mathbf{z}_j^t / \tau)}{\sum_k \exp((\mathbf{z}_i^v)^\top \mathbf{z}_k^t / \tau)} \quad (8)$$

$$= \frac{1}{\tau B} \sum_i \sum_j q_{ij} \left(-(\mathbf{z}_i^v)^\top \mathbf{z}_j^t + \tau \underbrace{\log \sum_k \exp((\mathbf{z}_i^v)^\top \mathbf{z}_k^t / \tau)}_{\text{LogSumExp (LSE)}} \right) \quad (9)$$

Since the feature embeddings are normalized, we have $\|\mathbf{z}_i^v\|_2 = \|\mathbf{z}_j^t\|_2 = 1$ and thus $(\mathbf{z}_i^v)^\top \mathbf{z}_j^t = 2 - \|\mathbf{z}_i^v - \mathbf{z}_j^t\|_2^2$. Moreover, following the scaled LogSumExp (LSE) rule, we can bound the right-side term as follows:

$$\max_k \{(\mathbf{z}_i^v)^\top \mathbf{z}_k^t\} < \tau LSE \leq \max_k \{(\mathbf{z}_i^v)^\top \mathbf{z}_k^t\} + \tau \log B \quad (10)$$

For a small τ (we use a value of 0.01 in our method), the bounds tighten and we get that

$$LSE \approx \frac{1}{\tau} \max_k \{(\mathbf{z}_i^v)^\top \mathbf{z}_k^t\} = \frac{1}{\tau} (\mathbf{z}_i^v)^\top \mathbf{z}_i^t \quad (11)$$

The last equality comes from the hypothesis that, in a well trained model, the maximum similarity occurs between the image and embedding of a samples and its corresponding text embedding. Our TTA loss can then be expressed as

$$\mathcal{L}_{\text{TTA}} \approx \frac{1}{\tau B} \left(\sum_i \sum_j q_{ij} \|\mathbf{z}_i^v - \mathbf{z}_j^t\|_2^2 + \sum_i (\mathbf{z}_i^v)^\top \mathbf{z}_i^t \right) + \text{const} \quad (12)$$

$$= \frac{1}{\tau B} \text{trace}((\mathbf{Z}^v)^\top (\mathbf{L}_Q + \mathbf{I}) \mathbf{Z}^t) + \text{const} \quad (13)$$

where \mathbf{I} is the identity matrix. The modified Laplacian $\mathbf{L}_Q + \mathbf{I}$ enforces nodes with a high connection weight (q_{ij}) to have similar embeddings, while also avoiding embeddings to collapse into a single vector. \square

	$K=1$	$K=3$	$K=4$
Original	89.80 \pm 0.05	90.04 \pm 0.13	90.41 \pm0.07
CIFAR 10.1	85.37 \pm 0.17	86.35 \pm0.27	86.07 \pm 0.21
C-Average	70.79	71.17	70.99

Table 2: Accuracy (%) on CIFAR-10, CIFAR-10.1 and CIFAR-10-C datasets with Level 5 corruption for different number of K selected classes to create pseudo-labels.

	$K=3$	$K=4$	$K=5$
3D	84.31	84.24	87.24
YT	82.80	83.17	83.46

Table 3: Accuracy (%) on the VisDA-C 3D training split (3D) and validation split (YT) with ViT-B/32 on different numbers of selected classes (K) to create pseudo-labels.

4 Experimental Settings

We evaluate CLIPArTT’s performance across diverse TTA datasets using established methodologies. These datasets simulate challenging domain shifts, offering insights into our approach’s efficacy. Additionally, we explore CLIPArTT’s adaptability on the original dataset through zero-shot test-time adaptation, crucial given the novel nature of the datasets. Our evaluation framework encompasses distinct categories, namely *natural images*, *common corruptions*, *simulated shift* and *video shift*, providing a comprehensive assessment of the model’s performance across diverse challenges.

In our evaluation of *natural images*, we utilize CIFAR-10, CIFAR-10.1, and CIFAR-100 datasets, each comprising 10,000 images and featuring 10 and 100 classes, respectively. These datasets represent natural imagery and are novel to the model under scrutiny. Notably, CIFAR-10.1 introduces a natural domain shift from CIFAR-10, thereby enriching our assessment with varied and nuanced data distributions.

Transitioning to our investigation of *common corruptions*, we turn to the CIFAR-10-C and CIFAR-100-C datasets Hendrycks and Dietterich [2019]. These datasets offer a diverse range of 15 distinct corruptions, including elastic transform and impulse noise, among others. Each corruption is characterized by 5 severity levels, yielding a total of 75 unique testing scenarios per dataset. Within each severity level, there are 10,000 images, contributing to a comprehensive evaluation of the model’s robustness against a variety of corruption types and intensities.

Furthermore, we examine the challenging VisDA-C dataset Peng et al. [2018], which represents two domain shifts: the *simulated shift* and *video shift*. The former comprises a set of 152,397 images rendered in 3D across 12 different classes. The later includes 72,372 YouTube video frames spanning the same categories. This dataset presents an important challenge, as it bridges the gap of the type of imagery that a model can be applied on.

Test-time adaptation. For test-time adaptation, model updates are applied to all the Layer Normalization (LN) layers within the visual encoder. We employ the ADAM optimizer with a fixed learning rate set to 10^{-3} . Throughout our experiments, a consistent batch size of 128 is utilized to maintain uniformity and enable effective comparisons across different scenarios. As in previous TTA works, a smaller learning rate of 10^{-4} is preferred to adapt on the 3D renderings split Vargas Hakim et al. [2023], as it represents a more aggressive shift.

Benchmarking. We compare the performance of CLIPArTT with *state-of-the-art* methods. Specifically, we utilize adapted versions of TENT Wang et al. [2021] and LAME Boudiaf et al. [2022] tailored to CLIP. The adapted TENT now updates only the affine parameters in Layer Normalization layers through entropy minimization directly on the similarity between image and text features, diverging from its original implementation (i.e., using classifier’s logits). Notably, we employ 10 iterations for TENT adaptation, a choice informed by our findings, as evidenced in Fig 2. For VisDA-C, we also explore using only 1 iteration, as in the original paper. Similarly, we utilize the image-to-text similarity scores as logits for LAME, where the Laplacian regularizer is applied to the similarity between image features. Finally, we extend the evaluation to include TPT Shu et al. [2022], a recent adaptation method for CLIP. TPT heavily relies on image augmentations, thus we reduce batch-size of 32 due to its high memory requirement.

5 Results

In this section, we outline the experimental outcomes derived from CLIPArTT and provide a comprehensive analysis. We first show a series of exploratory ablations that later help conduct the final experiments on the different datasets and compare with *state-of-the-art*.

5.1 Ablation Studies

Selection of the number of classes for new prompts. Determining the number of classes in building new prompts presents a critical aspect in our methodology. Table 13 illustrates various scenarios where $K = 3$ emerges as a favorable choice, exhibiting a remarkable accuracy of 100% across multiple instances of CIFAR-10 datasets. This initial observation is further corroborated by the findings presented in Table 14. However, the decision becomes more nuanced when applied to CIFAR-100 datasets. While leveraging the top 3 classes contributes to enhanced accuracy, it does not guarantee optimal performance. Similarly, adopting a strategy akin to CIFAR-10, wherein 30% of the classes are chosen, proves impractical due to resulting lengthy sentences that are impossible to tokenize. Examination of Table 4 reveals that the optimal choice varies depending on the distribution shift. Nonetheless, our analysis shows that $K = 3$ consistently yields superior performance, particularly evident in the average results across CIFAR-100-C. Consequently, we maintain $K = 3$ as the preferred configuration for all subsequent experiments on CIFAR datasets. A similar study was conducted for VisDA-C, in which $K = 5$ (See Table 3) is chosen as the number of classes.

	$K = 1$	$K = 3$	$K = 5$	$K = 7$	$K = 10$	$K = 20$
Original	69.00 \pm 0.22	69.79 \pm 0.04	69.68 \pm 0.07	69.56 \pm 0.02	69.78 \pm 0.02	69.93 \pm 0.08
Gaussian Noise	26.05 \pm 0.11	25.32 \pm 0.14	24.69 \pm 0.03	24.60 \pm 0.03	24.70 \pm 0.15	23.73 \pm 0.07
Shot noise	28.88 \pm 0.11	27.90 \pm 0.05	27.25 \pm 0.26	26.75 \pm 0.07	26.83 \pm 0.26	25.73 \pm 0.13
Impulse Noise	24.04 \pm 0.09	25.62 \pm 0.09	25.12 \pm 0.14	25.25 \pm 0.14	24.95 \pm 0.23	24.57 \pm 0.12
Defocus blur	49.03 \pm 0.15	49.88 \pm 0.23	49.75 \pm 0.11	49.74 \pm 0.25	49.62 \pm 0.10	49.49 \pm 0.07
Glass blur	26.77 \pm 0.14	27.89 \pm 0.03	27.76 \pm 0.23	27.28 \pm 0.07	26.57 \pm 0.07	25.52 \pm 0.09
Motion blur	46.50 \pm 0.09	47.93 \pm 0.14	47.48 \pm 0.21	47.57 \pm 0.10	47.53 \pm 0.09	47.36 \pm 0.09
Zoom blur	52.08 \pm 0.12	52.70 \pm 0.06	52.22 \pm 0.10	52.10 \pm 0.24	52.62 \pm 0.24	52.82 \pm 0.09
Snow	49.24 \pm 0.07	49.72 \pm 0.01	48.98 \pm 0.08	48.87 \pm 0.08	49.13 \pm 0.08	49.54 \pm 0.13
Frost	49.91 \pm 0.07	49.63 \pm 0.12	48.43 \pm 0.17	48.11 \pm 0.06	48.72 \pm 0.08	49.13 \pm 0.10
Fog	47.15 \pm 0.04	48.77 \pm 0.04	48.95 \pm 0.18	48.78 \pm 0.22	49.06 \pm 0.05	48.74 \pm 0.36
Brightness	60.01 \pm 0.08	61.27 \pm 0.08	60.77 \pm 0.16	60.89 \pm 0.19	60.98 \pm 0.18	61.03 \pm 0.19
Contrast	46.90 \pm 0.21	48.55 \pm 0.24	49.01 \pm 0.14	49.07 \pm 0.03	49.27 \pm 0.09	49.08 \pm 0.12
Elastic transform	36.32 \pm 0.10	37.45 \pm 0.08	37.63 \pm 0.12	37.31 \pm 0.09	37.13 \pm 0.16	36.94 \pm 0.11
Pixelate	32.52 \pm 0.17	33.88 \pm 0.14	34.40 \pm 0.15	34.38 \pm 0.16	34.65 \pm 0.09	34.32 \pm 0.02
JPEG compression	35.81 \pm 0.11	36.07 \pm 0.32	35.77 \pm 0.01	35.60 \pm 0.10	35.63 \pm 0.10	35.29 \pm 0.14
Average	40.75	41.51	41.21	41.09	41.16	40.89

Table 4: Accuracy (%) on CIFAR-100 and CIFAR-100-C datasets with Level 5 corruption for different number of K selected classes to create pseudo-labels.

Selection of the number of iterations. In line with our approach for TENT, we investigate optimal number of iterations. As demonstrated in Table 5, iterating 10 times strikes the most favorable balance, exhibiting superior performance across the overall average on CIFAR-10-C and yielding optimal results for numerous corruption types. Nonetheless, it is imperative to acknowledge that employing a lower number of iterations (e.g., Iter=5) may yield improved outcomes in scenarios with minimal or no distribution shift, while a higher number of iterations (e.g., Iter=20) may be more effective in mitigating severe distribution shifts. As a result, 10 iterations are used for all forthcoming experiments.

Pseudo-label selection for adaptation. For the target, we employed a linear combination of both image-to-image and text-to-text similarities to encapsulate the information derived from both modalities. This combination proved to be more effective than each modality separately (see Table 6). While selecting solely the text-to-text similarity for adaptation performs well, it falls short of achieving optimal results. Conversely, utilizing only the image-to-image similarity mainly improves for the original CIFAR-10 dataset and few corruption types.

Performance of the model for different batch-sizes. TTA methods have historically exhibited limitations when applied with small batch sizes. In our study, we investigate the performance of our model in this regard. As depicted in Table 15, performance improves significantly with increasing batch size. However, beyond a batch size of 8, no further performance gains are observed. This phenomenon can be attributed to the fact that, with smaller batch sizes, our method has the potential to introduce uncertainty by introducing multiple classes, thereby diminishing

	Iter = 1	Iter = 5	Iter = 10	Iter = 20
Original	89.59 \pm 0.01	90.54 \pm 0.09	90.04 \pm 0.13	88.32 \pm 0.12
CIFAR 10.1	84.78 \pm 0.02	86.67 \pm 0.06	86.35 \pm 0.27	84.33 \pm 0.31
Gaussian Noise	39.75 \pm 0.04	53.79 \pm 0.08	59.90 \pm 0.36	59.33 \pm 0.20
Shot noise	43.80 \pm 0.04	57.16 \pm 0.24	62.77 \pm 0.07	63.08 \pm 0.43
Impulse Noise	45.19 \pm 0.07	52.44 \pm 0.14	56.02 \pm 0.16	56.73 \pm 0.01
Defocus blur	72.93 \pm 0.07	76.36 \pm 0.10	76.74 \pm 0.05	75.33 \pm 0.13
Glass blur	46.61 \pm 0.06	57.45 \pm 0.13	61.77 \pm 0.16	62.01 \pm 0.27
Motion blur	67.89 \pm 0.03	74.34 \pm 0.14	76.01 \pm 0.19	75.94 \pm 0.28
Zoom blur	73.24 \pm 0.05	77.03 \pm 0.07	77.40 \pm 0.20	75.42 \pm 0.13
Snow	73.81 \pm 0.07	76.51 \pm 0.08	77.29 \pm 0.16	76.18 \pm 0.21
Frost	74.80 \pm 0.04	78.13 \pm 0.12	79.20 \pm 0.08	77.44 \pm 0.30
Fog	69.81 \pm 0.06	74.16 \pm 0.09	75.74 \pm 0.14	74.66 \pm 0.02
Brightness	84.16 \pm 0.01	86.61 \pm 0.10	86.59 \pm 0.16	85.14 \pm 0.42
Contrast	67.75 \pm 0.03	74.85 \pm 0.04	77.82 \pm 0.14	77.75 \pm 0.11
Elastic transform	63.15 \pm 0.08	68.53 \pm 0.19	70.20 \pm 0.01	68.48 \pm 0.24
Pixelate	54.20 \pm 0.02	61.87 \pm 0.04	66.52 \pm 0.13	67.13 \pm 0.15
JPEG compression	57.46 \pm 0.09	62.00 \pm 0.13	63.51 \pm 0.14	63.64 \pm 0.20
Average	62.30	68.75	71.17	70.55

Table 5: Accuracy (%) on CIFAR-10, CIFAR-10.1 and CIFAR-10-C datasets with Level 5 corruption for different number of iterations to update the model at test-time.

	Image	Text	Image + Text
Original	90.18 \pm 0.02	89.05 \pm 0.14	90.04 \pm 0.13
CIFAR 10.1	86.25 \pm 0.37	84.85 \pm 0.40	86.35 \pm 0.27
Gaussian Noise	59.05 \pm 0.30	59.29 \pm 0.27	59.90 \pm 0.36
Shot noise	62.11 \pm 0.18	61.89 \pm 0.31	62.77 \pm 0.07
Impulse Noise	55.43 \pm 0.12	55.48 \pm 0.10	56.02 \pm 0.16
Defocus blur	76.88 \pm 0.09	76.25 \pm 0.10	76.74 \pm 0.05
Glass blur	61.56 \pm 0.03	61.28 \pm 0.33	61.77 \pm 0.16
Motion blur	76.32 \pm 0.15	75.37 \pm 0.27	76.01 \pm 0.19
Zoom blur	77.66 \pm 0.09	76.29 \pm 0.11	77.40 \pm 0.20
Snow	77.28 \pm 0.08	76.03 \pm 0.16	77.29 \pm 0.16
Frost	78.80 \pm 0.18	78.05 \pm 0.21	79.20 \pm 0.08
Fog	75.69 \pm 0.17	73.70 \pm 0.15	75.74 \pm 0.14
Brightness	86.62 \pm 0.20	84.69 \pm 0.04	86.59 \pm 0.16
Contrast	77.43 \pm 0.12	74.52 \pm 0.02	77.82 \pm 0.14
Elastic transform	69.63 \pm 0.02	69.33 \pm 0.20	70.20 \pm 0.01
Pixelate	66.33 \pm 0.16	64.86 \pm 0.29	66.52 \pm 0.13
JPEG compression	63.92 \pm 0.13	63.44 \pm 0.20	63.51 \pm 0.14
Average	70.98	70.03	71.17

Table 6: Accuracy (%) on CIFAR-10, CIFAR-10.1 and CIFAR-10-C datasets with different targets.

	CLIP	BS = 8	BS = 16	BS = 32	BS = 64	BS = 128
Original	88.74	82.50 \pm 0.13	85.89 \pm 0.19	88.25 \pm 0.15	89.48 \pm 0.15	90.04 \pm 0.13
CIFAR 10.1	83.25	77.2 \pm 0.92	81.55 \pm 0.53	84.00 \pm 0.31	85.40 \pm 0.08	86.35 \pm 0.27
C-Average	59.22	61.10	64.72	67.70	69.82	71.17

Table 7: Accuracy (%) on CIFAR-10, CIFAR-10.1 and CIFAR-10-C datasets with Level 5 corruption for different number of batch-size.

performance, especially when the model is already confident. In subsequent experiments, we maintain a batch size of 128, consistent with prevailing practices in the *state-of-the-art* methodologies.

5.2 Experiments

	CLIP	LAME	TENT	TPT (BS=32)	CLIPArTT
Original	88.74	89.36 ±0.06	91.69 ±0.10	88.06 ±0.06	90.04 ±0.13
CIFAR 10.1	83.25	81.22 ±0.33	87.60 ±0.45	81.80 ±0.27	86.35 ±0.27
Gaussian Noise	35.27	24.71 ±0.11	41.27 ±0.27	33.90 ±0.08	59.90 ±0.36
Shot noise	39.67	27.44 ±0.09	47.20 ±0.23	38.20 ±0.02	62.77 ±0.07
Impulse Noise	42.61	31.38 ±0.15	48.58 ±0.31	37.66 ±0.20	56.02 ±0.16
Defocus blur	69.76	62.45 ±0.44	77.12 ±0.16	67.83 ±0.28	76.74 ±0.05
Glass blur	42.40	29.96 ±0.06	52.65 ±0.30	38.81 ±0.12	61.77 ±0.16
Motion blur	63.97	54.00 ±0.36	71.25 ±0.09	63.39 ±0.13	76.01 ±0.19
Zoom blur	69.83	61.97 ±0.36	76.20 ±0.19	68.95 ±0.16	77.40 ±0.20
Snow	71.78	64.61 ±0.48	78.29 ±0.20	70.16 ±0.10	77.29 ±0.16
Frost	72.86	65.17 ±0.17	79.84 ±0.09	72.39 ±0.22	79.20 ±0.08
Fog	67.04	59.13 ±0.49	77.39 ±0.01	64.31 ±0.28	75.74 ±0.14
Brightness	81.87	80.05 ±0.23	87.78 ±0.03	81.30 ±0.18	86.59 ±0.16
Contrast	64.37	56.91 ±0.37	79.47 ±0.11	62.26 ±0.31	77.82 ±0.14
Elastic transform	60.83	53.89 ±0.20	70.00 ±0.25	56.43 ±0.27	70.20 ±0.01
Pixelate	50.53	39.67 ±0.34	63.74 ±0.18	42.80 ±0.40	66.52 ±0.13
JPEG compression	55.48	47.24 ±0.14	62.64 ±0.14	53.67 ±0.25	63.51 ±0.14
Average	59.22	50.57	67.56	56.80	71.17

Table 8: Accuracy (%) on CIFAR-10, CIFAR-10.1 and CIFAR-10-C datasets with ViT-B/32 as visual encoder.

Performance analysis under natural or no domain shift. In the different Tables 8, 9, 10, and 11, CLIPArTT consistently enhances accuracy across CIFAR-10, CIFAR10.1, and CIFAR-100 datasets compared to the baseline (+2%, +3%, +8% respectively with ViT-B/32). This improvement suggests that even datasets devoid of corruption, which may not have been seen by the model during training, can benefit from adaptation. Consequently, a zero-shot model can leverage adaptation at test-time, relying solely on the model’s predictions. However, while CLIPArTT outperforms the baseline, as well as LAME and TPT with this fixed version, it is worth noting that TENT may yield superior results depending on the visual encoder and the number of classes. Entropy minimization used solely on confident results proves to be also effective. Interestingly, the corruptions in which TENT achieves a better performance tend to already have higher accuracy values.

	CLIP	LAME	TENT	TPT (BS=32)	CLIPArTT
Original	61.68	58.27 ±0.17	69.74 ±0.16	63.78 ±0.28	69.79 ±0.04
Gaussian Noise	14.80	12.72 ±0.04	14.38 ±0.14	14.03 ±0.10	25.32 ±0.14
Shot noise	16.03	13.78 ±0.08	17.34 ±0.27	15.25 ±0.17	27.90 ±0.05
Impulse Noise	13.85	7.82 ±0.14	10.03 ±0.13	13.01 ±0.13	25.62 ±0.09
Defocus blur	36.74	33.38 ±0.11	49.05 ±0.07	37.60 ±0.17	49.88 ±0.23
Glass blur	14.19	9.00 ±0.05	3.71 ±0.07	16.41 ±0.02	27.89 ±0.03
Motion blur	36.14	32.79 ±0.13	46.62 ±0.27	37.52 ±0.23	47.93 ±0.14
Zoom blur	40.24	37.57 ±0.15	51.84 ±0.15	42.99 ±0.11	52.70 ±0.06
Snow	38.95	35.49 ±0.18	46.71 ±0.21	42.35 ±0.13	49.72 ±0.01
Frost	40.56	37.22 ±0.21	44.90 ±0.27	43.31 ±0.14	49.63 ±0.12
Fog	38.00	35.94 ±0.09	47.31 ±0.04	38.81 ±0.17	48.77 ±0.04
Brightness	48.18	44.93 ±0.08	60.58 ±0.18	50.23 ±0.11	61.27 ±0.08
Contrast	29.53	27.52 ±0.06	45.90 ±0.11	28.09 ±0.09	48.55 ±0.24
Elastic transform	26.33	24.01 ±0.02	33.09 ±0.08	28.12 ±0.15	37.45 ±0.08
Pixelate	21.98	19.55 ±0.13	26.47 ±0.09	20.43 ±0.14	33.88 ±0.14
JPEG compression	25.91	21.77 ±0.14	29.89 ±0.07	28.82 ±0.09	36.07 ±0.32
Average	29.43	26.23	35.19	30.46	41.51

Table 9: Accuracy (%) on CIFAR-100 and CIFAR-100-C datasets with ViT-B/32 as visual encoder.

Performance analysis under common corruptions. In the various referenced tables, including Tables 8, 9, 10, and 11, CLIPArTT consistently outperforms the baseline, TPT, and LAME across all visual encoders, resulting in

		CLIP	TENT	TPT (BS=32)	CLIPArTT
Original	ViT-B/16	89.25	92.75 ± 0.17	89.80 ± 0.05	92.61 ± 0.05
	ViT-L/14	95.36	96.13 ± 0.06	95.18 ± 0.02	95.16 ± 0.03
CIFAR-10.1	ViT-B/16	84.00	88.52 ± 0.33	83.75 ± 0.21	88.72 ± 0.33
	ViT-L/14	91.20	92.22 ± 0.25	91.32 ± 0.12	91.02 ± 0.02
C-Average	ViT-B/16	60.15	68.00	59.75	73.22
	ViT-L/14	76.04	79.18	75.01	78.06

Table 10: Accuracy (%) on CIFAR-10, CIFAR-10.1 and CIFAR-10-C datasets with ViT-B/16 and ViT-L/14 as visual encoders.

		CLIP	TENT	TPT (BS=32)	CLIPArTT
Original	ViT-B/16	64.76	71.73 ± 0.14	67.15 ± 0.23	71.34 ± 0.07
	ViT-L/14	73.28	78.03 ± 0.08	76.85 ± 0.06	79.42 ± 0.08
C-Average	ViT-B/16	32.01	37.90	33.73	40.08
	ViT-L/14	44.59	50.14	47.58	52.52

Table 11: Accuracy (%) on CIFAR-100 and CIFAR-100-C datasets with ViT-B/16 and ViT-L/14 as visual encoders.

enhancements of up to 13% on average. A more detailed examination reveals that CLIPArTT frequently surpasses TENT, particularly in instances where the baseline performs poorly. This observation implies that CLIPArTT consistently outperforms TENT, which tends to compromise the model’s performance under conditions of low baseline confidence. For instance, in Table 9, TENT experiences a 3% decrease compared to the baseline under *Impulse Noise*, while CLIPArTT exhibits a 12% improvement. Conversely, when the baseline is confident, CLIPArTT consistently maintains a high performance. As an illustration, Table 8 shows that while CLIP achieves an accuracy of 81.87% under *Brightness* corruption, both TENT and CLIPArTT contribute to improvements of 7% and 6%, respectively.

Performance analysis under simulated and video shifts. Results on the 3D and YT splits of VisDA-C are shown in Table 12. With respect to pure CLIP, our method achieves an important improvement of accuracy with the three different image encoders. CLIPArTT also achieves a competitive advantage against TENT, LAME and TPT. We observed however that using TENT with 10 iterations (here named TENT-10) is a strong contender, achieving practically the same score on 3D images and outperforming on YouTube frames by a small margin. This can mean that TENT’s entropy minimization can achieve faster improvement with certain domain shifts.

6 Conclusions

In this study, we introduce CLIPArTT, the first comprehensive Test-Time Adaptation framework designed specifically for Vision-Language Models. By leveraging the model’s predictions as new pseudo-labels, we effectively minimize cross-entropy loss at test-time, thereby enhancing model performance even within a zero-shot setting. To ensure fair comparisons, we also incorporate Test-Time Adaptation models into this new benchmark for VLMs.

A comprehensive ablation study is conducted to determine optimal hyperparameters and gain deeper insights into the various model configurations. Our experimental results demonstrate that CLIPArTT achieves highly competitive performance across TTA datasets, surpassing *state-of-the-art* approaches. While TENT remains a strong competitor,

		CLIP	TENT	TENT-10	LAME	TPT (BS=32)	CLIPArTT
3D	ViT-B/16	87.04	87.15 ± 0.21	88.08 ± 0.05	85.83 ± 0.06	83.85 ± 0.06	88.01 ± 0.47
	ViT-B/32	84.51	84.75 ± 0.17	85.82 ± 0.02	83.85 ± 0.03	78.45 ± 0.05	87.24 ± 0.04
	ViT-L/14	90.62	90.93 ± 0.01	91.33 ± 0.01	90.15 ± 0.07	91.07 ± 0.05	91.18 ± 0.01
YT	ViT-B/16	86.71	86.96 ± 0.02	87.44 ± 0.02	86.24 ± 0.0	85.69 ± 0.05	86.22 ± 0.01
	ViT-B/32	84.45	84.72 ± 0.01	85.46 ± 0.02	84.41 ± 0.02	82.95 ± 0.01	83.46 ± 0.03
	ViT-L/14	84.93	85.38 ± 0.01	86.65 ± 0.05	85.08 ± 0.04	85.54 ± 0.38	85.55 ± 0.01

Table 12: Accuracy (%) on the VisDA-C training split (3D) and validation split (YT) with the three different feature extractors.

our model offers enhanced versatility by effectively addressing both natural and severe domain shifts, thus exhibiting robustness across various scenarios.

Exploring the potential of text prompts in classification represents a promising avenue for future research. Investigating alternative methods to fine-tune these text prompts could yield valuable insights. Moreover, extending the study of Test-Time Adaptation to other scenarios, such as segmentation or object detection with Vision-Language Models (VLMs), holds significant promise for advancing our understanding of model adaptability and performance across diverse tasks.

CLIPArTT: Light-weight Adaptation of CLIP to New Domains at Test Time – Supplementary Material

A Unsupervised clustering

In Fig. 3, tSNE visualizations of data points are shown. We show how the distribution of data points change after adaptation, which improves the accuracy of class predictions and facilitates the assignment of ground truth labels.

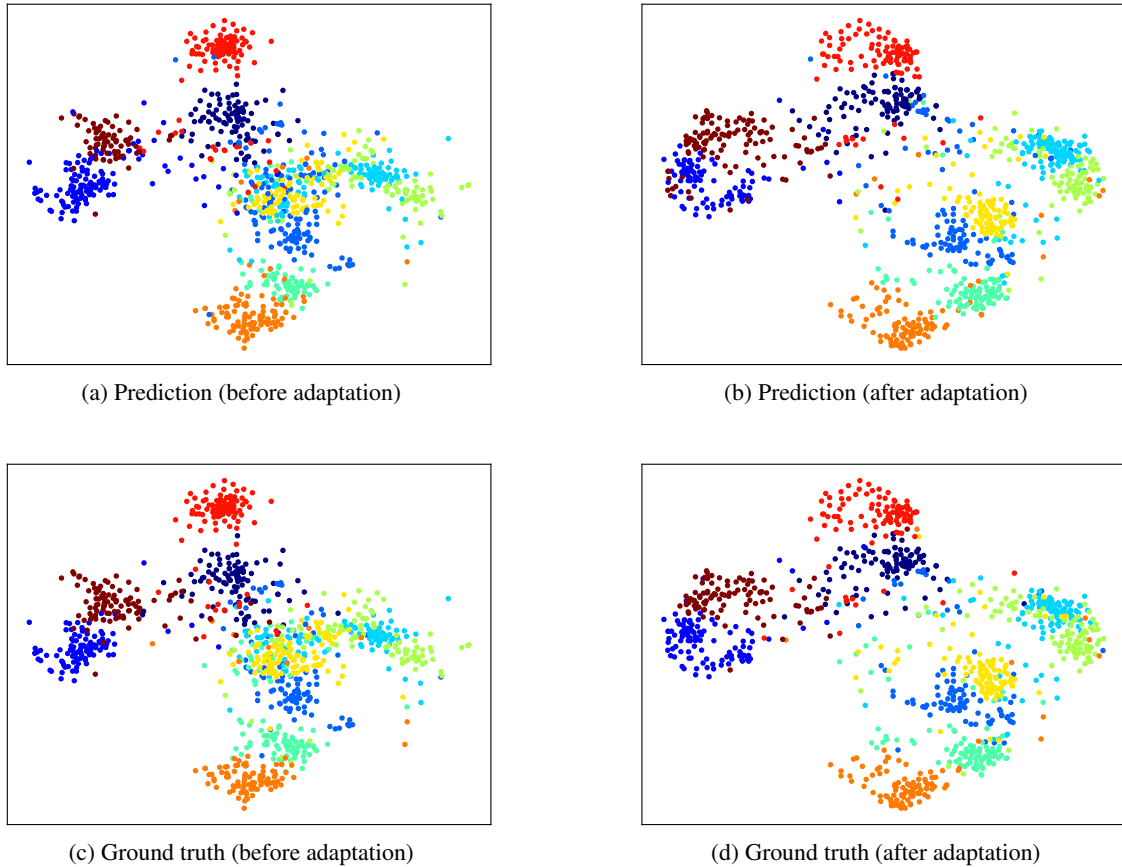


Figure 3: The t-SNE visualizations exhibit discernible attributes of brightness within the visual features derived from CLIPArTT. Panels (a) and (b) present the model’s predictions before and after 10 iterations of adaptation, respectively. Panels (c) and (d) demonstrate the actual labels in the absence of adaptation and following adaptation of the representations, respectively.

B Evolution of similarity matrices

A fundamental component of CLIPArTT is the employment of image-to-image and text-to-text similarity matrices to build new pseudo labels. In Fig. 4, we show an example of a batch of five images. While the largest image-to-image similarity values concentrate on the main diagonal, the text-to-text similarity using the K most confident classes for the new text prompt, highly impacts the correlation between images and text (CLIPArTT logits).

C Comprehensive experimental results

We present comprehensive tables containing all the detailed information about results that was summarized in the main paper.

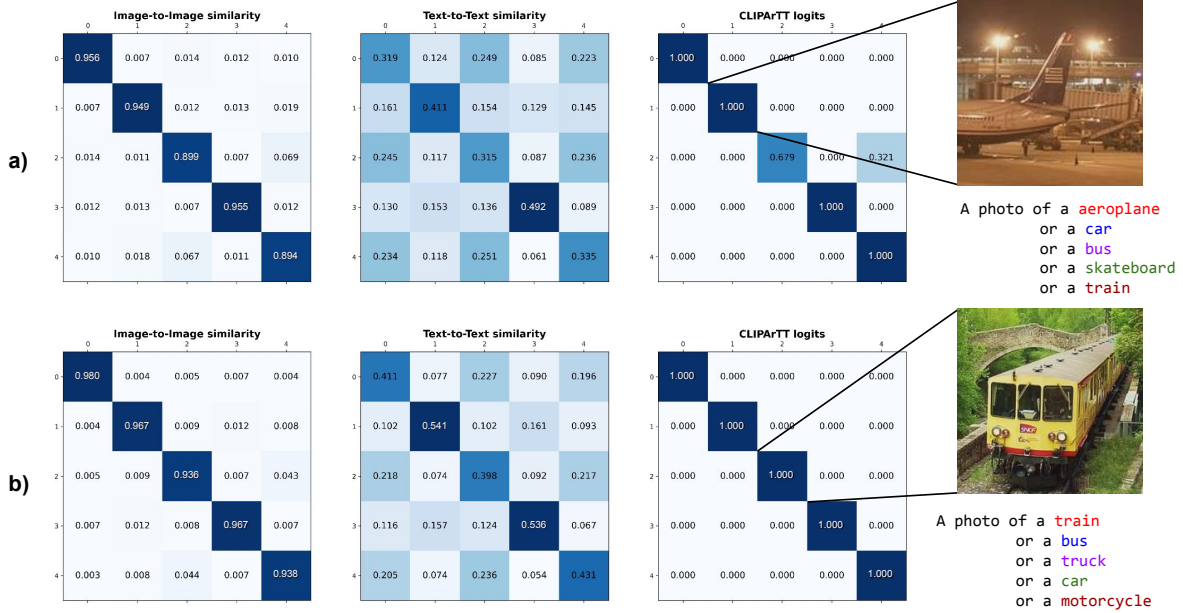


Figure 4: Similarity matrices before (a) and after (b) adaptation using $K = 5$ classes. There is an increase in the confidence of the logits when using a pseudolabel from the new prompt with the K most confident classes.

	CIFAR10		CIFAR100	
	Top 1	Top 3	Top 1	Top 3
ORIGINAL	88.74	100.00	61.68	97.34
Gaussian Noise	35.27	99.87	14.8	63.66
Shot noise	39.67	99.99	16.03	67.02
Impulse Noise	42.61	100.00	13.85	64.4
Defocus blur	69.76	100.00	36.74	90.14
Glass blur	42.40	100.00	14.19	61.66
Motion blur	63.97	100.00	36.14	90.36
Zoom blur	69.83	100.00	40.24	91.27
Snow	71.78	100.00	38.95	91.40
Frost	72.86	100.00	40.56	92.23
Fog	67.04	99.98	38.00	91.51
Brightness	81.87	100.00	48.18	93.10
Contrast	64.37	100.00	29.53	84.67
Elastic transform	60.83	100.00	26.33	78.96
Pixelate	50.53	100.00	21.98	75.65
JPEG compression	55.48	100.00	25.91	80.81
Average	59.22	99.99	29.43	81.12

Table 13: Accuracy (%) on CIFAR-10/100 and CIFAR-10/100-C datasets with Level 5 corruption for the top 1 or the top 3 predicted classes.

References

- Alec Radford, Jong Wook Kim, Chris Hallacy, Aditya Ramesh, Gabriel Goh, Sandhini Agarwal, Girish Sastry, Amanda Askell, Pamela Mishkin, Jack Clark, et al. Learning transferable visual models from natural language supervision. In *International conference on machine learning*, pages 8748–8763. PMLR, 2021.
- Chao Jia, Yinfei Yang, Ye Xia, Yi-Ting Chen, Zarana Parekh, Hieu Pham, Quoc Le, Yun-Hsuan Sung, Zhen Li, and Tom Duerig. Scaling up visual and vision-language representation learning with noisy text supervision. In *International conference on machine learning*, pages 4904–4916. PMLR, 2021.

	K = 1	K = 3	K = 4
ORIGINAL	89.8 \pm 0.05	90.04 \pm 0.13	90.41 \pm 0.07
CIFAR 10.1	85.37 \pm 0.17	86.35 \pm 0.27	86.07 \pm 0.21
Gaussian Noise	60.2 \pm 0.24	59.90 \pm 0.36	59.71 \pm 0.15
Shot noise	62.08 \pm 0.11	62.77 \pm 0.07	62.17 \pm 0.16
Impulse Noise	54.33 \pm 0.07	56.02 \pm 0.16	56.27 \pm 0.15
Defocus blur	77.16 \pm 0.02	76.74 \pm 0.05	76.79 \pm 0.11
Glass blur	61.91 \pm 0.15	61.77 \pm 0.16	61.72 \pm 0.23
Motion blur	74.94 \pm 0.15	76.01 \pm 0.19	76.33 \pm 0.1
Zoom blur	76.84 \pm 0.13	77.40 \pm 0.20	77.15 \pm 0.04
Snow	76.87 \pm 0.05	77.29 \pm 0.16	76.56 \pm 0.16
Frost	77.81 \pm 0.04	79.20 \pm 0.08	78.42 \pm 0.04
Fog	75.83 \pm 0.28	75.74 \pm 0.14	75.65 \pm 0.06
Brightness	85.55 \pm 0.12	86.59 \pm 0.16	86.83 \pm 0.1
Contrast	78.02 \pm 0.18	77.82 \pm 0.14	78.27 \pm 0.14
Elastic transform	69.42 \pm 0.07	70.20 \pm 0.01	69.81 \pm 0.2
Pixelate	66.07 \pm 0.09	66.52 \pm 0.13	66.45 \pm 0.08
JPEG compression	64.82 \pm 0.26	63.51 \pm 0.14	62.72 \pm 0.25
Average	70.79	71.17	70.99

Table 14: Accuracy (%) on CIFAR-10, CIFAR-10.1 and CIFAR-10-C datasets with Level 5 corruption for different number of K selected classes to create pseudo-label.

	CLIP	BS = 8	BS = 16	BS = 32	BS = 64	BS = 128
ORIGINAL	88.74	82.50 \pm 0.13	85.89 \pm 0.19	88.25 \pm 0.15	89.48 \pm 0.15	90.04 \pm 0.13
CIFAR 10.1	83.25	77.2 \pm 0.92	81.55 \pm 0.53	84.00 \pm 0.31	85.40 \pm 0.08	86.35 \pm 0.27
Gaussian Noise	35.27	47.30 \pm 0.37	50.91 \pm 0.35	54.23 \pm 0.28	57.89 \pm 0.13	59.90 \pm 0.36
Shot noise	39.67	49.62 \pm 0.26	53.1 \pm 0.27	56.88 \pm 0.23	60.56 \pm 0.12	62.77 \pm 0.07
Impulse Noise	42.61	47.24 \pm 0.22	50.24 \pm 0.48	52.7 \pm 0.21	54.88 \pm 0.17	56.02 \pm 0.16
Defocus blur	69.76	68.24 \pm 0.35	72.22 \pm 0.04	75.09 \pm 0.16	75.97 \pm 0.27	76.74 \pm 0.05
Glass blur	42.40	49.49 \pm 0.30	53.27 \pm 0.04	57.18 \pm 0.24	60.12 \pm 0.14	61.77 \pm 0.16
Motion blur	63.97	65.22 \pm 0.06	69.02 \pm 0.30	72.54 \pm 0.27	74.71 \pm 0.18	76.01 \pm 0.19
Zoom blur	69.83	67.69 \pm 0.20	71.33 \pm 0.11	74.53 \pm 0.11	76.35 \pm 0.07	77.40 \pm 0.20
Snow	71.78	68.68 \pm 0.42	72.37 \pm 0.11	74.93 \pm 0.18	76.53 \pm 0.41	77.29 \pm 0.16
Frost	72.86	70.35 \pm 0.25	73.93 \pm 0.34	76.81 \pm 0.23	78.22 \pm 0.13	79.20 \pm 0.08
Fog	67.04	66.25 \pm 0.31	69.71 \pm 0.24	72.36 \pm 0.23	73.96 \pm 0.21	75.74 \pm 0.14
Brightness	81.87	77.36 \pm 0.17	81.20 \pm 0.20	84.07 \pm 0.08	85.58 \pm 0.25	86.59 \pm 0.16
Contrast	64.37	65.12 \pm 0.07	69.02 \pm 0.12	72.60 \pm 0.46	75.79 \pm 0.24	77.82 \pm 0.14
Elastic transform	60.83	59.61 \pm 0.11	63.67 \pm 0.13	66.36 \pm 0.26	68.74 \pm 0.07	70.20 \pm 0.01
Pixelate	50.53	56.78 \pm 0.24	60.01 \pm 0.06	62.57 \pm 0.19	64.64 \pm 0.03	66.52 \pm 0.13
JPEG compression	55.48	57.59 \pm 0.26	60.78 \pm 0.12	62.63 \pm 0.06	63.43 \pm 0.16	63.51 \pm 0.14
Average	59.22	61.10	64.72	67.70	69.82	71.17

Table 15: Accuracy (%) on CIFAR-10, CIFAR-10.1 and CIFAR-10-C datasets with Level 5 corruption for different batch sizes.

Alexander Kirillov, Eric Mintun, Nikhila Ravi, Hanzi Mao, Chloe Rolland, Laura Gustafson, Tete Xiao, Spencer Whitehead, Alexander C Berg, Wan-Yen Lo, et al. Segment anything. *arXiv preprint arXiv:2304.02643*, 2023.

Ziyi Lin, Shijie Geng, Renrui Zhang, Peng Gao, Gerard de Melo, Xiaogang Wang, Jifeng Dai, Yu Qiao, and Hongsheng Li. Frozen clip models are efficient video learners. In *European Conference on Computer Vision*, pages 388–404. Springer, 2022.

	CLIP	TENT	TPT (BS=32)	CLIPArTT
ORIGINAL	89.25	92.75 ± 0.17	89.80 ± 0.05	92.61 ± 0.05
CIFAR 10.1	84.00	88.52 ± 0.33	83.75.0.21 \pm	88.72 ± 0.33
Gaussian Noise	37.75	31.04 ± 0.38	35.35 ± 0.15	60.89 ± 0.26
Shot noise	41.10	40.54 ± 0.41	41.03 ± 0.19	65.19 ± 0.21
Impulse Noise	51.71	58.03 ± 0.16	54.86 ± 0.07	67.55 ± 0.09
Defocus blur	70.07	77.57 ± 0.03	70.29 ± 0.02	78.92 ± 0.12
Glass blur	42.24	47.16 ± 0.05	37.86 ± 0.17	57.18 ± 0.20
Motion blur	65.81	76.16 ± 0.05	67.43 ± 0.11	76.59 ± 0.06
Zoom blur	72.50	79.64 ± 0.12	72.91 ± 0.02	79.62 ± 0.11
Snow	73.23	81.68 ± 0.03	72.98 ± 0.32	81.13 ± 0.29
Frost	76.52	83.22 ± 0.05	75.87 ± 0.16	81.24 ± 0.08
Fog	68.35	80.78 ± 0.15	69.13 ± 0.27	78.47 ± 0.19
Brightness	83.36	89.85 ± 0.11	83.67 ± 0.14	88.66 ± 0.15
Contrast	61.90	79.24 ± 0.19	62.16 ± 0.06	75.15 ± 0.07
Elastic transform	53.16	62.54 ± 0.08	51.26 ± 0.23	69.49 ± 0.08
Pixelate	48.48	67.08 ± 0.24	44.65 ± 0.21	71.80 ± 0.16
JPEG compression	56.05	65.42 ± 0.05	56.73 ± 0.07	66.42 ± 0.25
Average	60.15	68.00	59.75	73.22

Table 16: Accuracy (%) on CIFAR-10, CIFAR-10.1 and CIFAR-10-C datasets with ViT-B/16 as visual encoder.

	CLIP	TENT	TPT (BS=32)	CLIPArTT
ORIGINAL	95.36	96.13 ± 0.06	95.18 ± 0.02	95.16 ± 0.03
CIFAR 10.1	91.20	92.22 ± 0.25	91.32 ± 0.12	91.02 ± 0.02
Gaussian Noise	64.64	68.87 ± 0.20	64.44 ± 0.11	70.04 ± 0.31
Shot noise	67.82	71.95 ± 0.06	66.81 ± 0.19	71.44 ± 0.16
Impulse Noise	78.21	80.22 ± 0.19	76.46 ± 0.17	79.42 ± 0.15
Defocus blur	80.73	83.10 ± 0.03	79.01 ± 0.23	81.75 ± 0.19
Glass blur	50.29	57.12 ± 0.07	49.64 ± 0.23	58.13 ± 0.23
Motion blur	80.75	82.69 ± 0.11	78.85 ± 0.04	80.76 ± 0.12
Zoom blur	82.75	84.91 ± 0.08	82.32 ± 0.13	83.39 ± 0.05
Snow	83.01	85.99 ± 0.11	82.69 ± 0.10	84.48 ± 0.07
Frost	84.90	87.15 ± 0.12	84.63 ± 0.08	85.21 ± 0.06
Fog	78.44	81.30 ± 0.07	77.56 ± 0.17	79.27 ± 0.07
Brightness	91.67	93.07 ± 0.04	90.94 ± 0.04	91.87 ± 0.09
Contrast	84.20	87.93 ± 0.04	82.88 ± 0.09	86.19 ± 0.06
Elastic transform	65.45	69.96 ± 0.12	64.81 ± 0.14	67.43 ± 0.24
Pixelate	75.10	77.89 ± 0.05	72.92 ± 0.12	77.11 ± 0.10
JPEG compression	72.58	75.49 ± 0.07	71.18 ± 0.19	74.46 ± 0.11
Average	76.04	79.18	75.01	78.06

Table 17: Accuracy (%) on CIFAR-10, CIFAR-10.1 and CIFAR-10-C datasets with ViT-L/14 as visual encoder.

Andrey Guzhov, Federico Raue, Jörn Hees, and Andreas Dengel. Audioclip: Extending clip to image, text and audio. In *ICASSP 2022-2022 IEEE International Conference on Acoustics, Speech and Signal Processing (ICASSP)*, pages 976–980. IEEE, 2022.

Jie Liu, Yixiao Zhang, Jie-Neng Chen, Junfei Xiao, Yongyi Lu, Bennett A Landman, Yixuan Yuan, Alan Yuille, Yucheng Tang, and Zongwei Zhou. Clip-driven universal model for organ segmentation and tumor detection. In *Proceedings of the IEEE/CVF International Conference on Computer Vision*, pages 21152–21164, 2023.

Zhengfeng Lai, Noranart Vesdapunt, Ning Zhou, Jun Wu, Cong Phuoc Huynh, Xuelu Li, Kah Kuen Fu, and Chen-Nee Chuah. Padclip: Pseudo-labeling with adaptive debiasing in clip for unsupervised domain adaptation. In *Proceedings of the IEEE/CVF International Conference on Computer Vision (ICCV)*, pages 16155–16165, October 2023.

Manli Shu, Weili Nie, De-An Huang, Zhiding Yu, Tom Goldstein, Anima Anandkumar, and Chaowei Xiao. Test-time prompt tuning for zero-shot generalization in vision-language models. In S. Koyejo, S. Mohamed, A. Agar-

	CLIP	TENT	TPT (BS=32)	CLIPArTT
ORIGINAL	64.76	71.73 ±0.14	67.15 ±0.23	71.34 ±0.07
Gaussian Noise	15.88	12.28 ±0.20	15.43 ±0.03	19.01 ±0.24
Shot noise	17.49	15.07 ±0.21	16.88 ±0.07	20.27 ±0.21
Impulse Noise	21.43	13.13 ±0.16	22.12 ±0.15	17.66 ±0.10
Defocus blur	40.10	50.35 ±0.03	41.08 ±0.22	49.86 ±0.13
Glass blur	13.48	4.84 ±0.14	18.43 ±0.15	18.34 ±0.31
Motion blur	39.82	49.85 ±0.37	40.85 ±0.26	50.00 ±0.09
Zoom blur	45.45	54.76 ±0.04	46.77 ±0.06	54.13 ±0.08
Snow	42.77	52.38 ±0.18	47.24 ±0.18	52.80 ±0.27
Frost	45.39	51.66 ±0.04	48.61 ±0.14	49.56 ±0.08
Fog	38.98	50.74 ±0.14	39.92 ±0.16	49.92 ±0.11
Brightness	52.55	64.26 ±0.09	55.83 ±0.10	63.76 ±0.13
Contrast	33.32	48.69 ±0.08	33.13 ±0.16	47.86 ±0.02
Elastic transform	24.39	33.56 ±0.28	27.36 ±0.10	32.93 ±0.23
Pixelate	21.89	36.20 ±0.28	21.26 ±0.10	39.49 ±0.21
JPEG compression	27.21	30.80 ±0.05	30.97 ±0.10	35.56 ±0.23
Average	32.01	37.90	33.73	40.08

Table 18: Accuracy (%) on CIFAR-100 and CIFAR-100-C datasets with ViT-B/16 as visual encoder.

	CLIP	TENT	TPT (BS=16)	CLIPArTT
ORIGINAL	73.28	78.03 ±0.08	76.85 ±0.06	79.42 ±0.08
Gaussian Noise	30.55	36.93 ±0.03	36.10 ±0.11	41.46 ±0.15
Shot noise	34.58	40.96 ±0.16	38.23 ±0.13	44.27 ±0.09
Impulse Noise	44.89	49.09 ±0.14	49.69 ±0.21	51.44 ±0.23
Defocus blur	48.88	55.23 ±0.07	50.43 ±0.19	56.55 ±0.22
Glass blur	23.46	27.02 ±0.23	24.35 ±0.22	30.47 ±0.14
Motion blur	50.83	56.03 ±0.20	51.94 ±0.04	56.98 ±0.18
Zoom blur	56.02	61.19 ±0.10	56.96 ±0.16	62.56 ±0.04
Snow	49.03	55.60 ±0.09	54.89 ±0.11	58.81 ±0.11
Frost	53.27	58.21 ±0.15	58.15 ±0.33	60.38 ±0.23
Fog	48.51	53.37 ±0.25	49.26 ±0.13	54.38 ±0.04
Brightness	60.53	67.34 ±0.17	66.60 ±0.10	69.63 ±0.14
Contrast	50.24	59.91 ±0.13	53.64 ±0.24	63.39 ±0.13
Elastic transform	35.07	38.49 ±0.12	35.72 ±0.09	39.57 ±0.39
Pixelate	43.86	48.37 ±0.17	44.32 ±0.10	50.45 ±0.16
JPEG compression	39.11	44.42 ±0.09	43.44 ±0.11	47.45 ±0.14
Average	44.59	50.14	47.58	52.52

Table 19: Accuracy (%) on CIFAR-100 and CIFAR-100-C datasets with ViT-L/14 as visual encoder.

wal, D. Belgrave, K. Cho, and A. Oh, editors, *Advances in Neural Information Processing Systems*, volume 35, pages 14274–14289. Curran Associates, Inc., 2022. URL https://proceedings.neurips.cc/paper_files/paper/2022/file/5bf2b802e24106064dc547ae9283bb0c-Paper-Conference.pdf.

Zachary Nado, Shreyas Padhy, D. Sculley, Alexander D’Amour, Balaji Lakshminarayanan, and Jasper Snoek. Evaluating prediction-time batch normalization for robustness under covariate shift. *arXiv:2006.10963 [cs, stat]*, January 2021. URL <http://arxiv.org/abs/2006.10963>. arXiv: 2006.10963.

Dequan Wang, Evan Shelhamer, Shaoteng Liu, Bruno Olshausen, and Trevor Darrell. Tent: Fully test-time adaptation by entropy minimization. 2021. URL <https://openreview.net/forum?id=uXl3bZLkr3c>.

Sachin Goyal, Mingjie Sun, Aditi Raghunathan, and Zico Kolter. Test-time adaptation via conjugate pseudo-labels. *Advances in Neural Information Processing Systems*, 2022.

Marvin Zhang, Sergey Levine, and Chelsea Finn. Memo: Test time robustness via adaptation and augmentation. In S. Koyejo, S. Mohamed, A. Agarwal, D. Belgrave, K. Cho, and A. Oh, editors, *Advances in Neural Information Processing Systems*, volume 35, pages 38629–38642. Curran Associates, Inc., 2022. URL https://proceedings.neurips.cc/paper_files/paper/2022/file/fc28053a08f59fccb48b11f2e31e81c7-Paper-Conference.pdf.

- Guoliang Lin, Hanjiang Lai, Yan Pan, and Jian Yin. Improving entropy-based test-time adaptation from a clustering view. *arXiv preprint arXiv:2310.20327*, 2023.
- Jungsoo Lee, Debasmit Das, Jaegul Choo, and Sungha Choi. Towards open-set test-time adaptation utilizing the wisdom of crowds in entropy minimization. In *Proceedings of the IEEE/CVF International Conference on Computer Vision (ICCV)*, pages 16380–16389, October 2023.
- Jian Liang, Dapeng Hu, and Jiashi Feng. Do we really need to access the source data? source hypothesis transfer for unsupervised domain adaptation. 2020.
- Qin Wang, Olga Fink, Luc Van Gool, and Dengxin Dai. Continual test-time domain adaptation. In *Proceedings of the IEEE/CVF Conference on Computer Vision and Pattern Recognition*, pages 7201–7211, 2022.
- Qilong Wu, Xiangyu Yue, and Alberto Sangiovanni-Vincentelli. Domain-agnostic test-time adaptation by prototypical training with auxiliary data. In *NeurIPS 2021 Workshop on Distribution Shifts: Connecting Methods and Applications*, 2021.
- Malik Boudiaf, Romain Mueller, Ismail Ben Ayed, and Luca Bertinetto. Parameter-free online test-time adaptation. In *IEEE/CVF Conference on Computer Vision and Pattern Recognition (CVPR)*, pages 8344–8353, 2022.
- Yu Sun, Xiaolong Wang, Zhuang Liu, John Miller, Alexei A. Efros, and Moritz Hardt. Test-time training with self-supervision for generalization under distribution shifts. In *International Conference on Machine Learning (ICML)*, 2020.
- Yuejiang Liu, Parth Kothari, Bastien van Delft, Baptiste Bellot-Gurlet, Taylor Mordan, and Alexandre Alahi. Ttt++: When does self-supervised test-time training fail or thrive? *Neural Information Processing Systems (NeurIPS)*, 2021.
- David Osowiechi, Gustavo A. Vargas Hakim, Mehrdad Noori, Milad Cheraghalikhani, Ismail Ayed, and Christian Desrosiers. Tttflow: Unsupervised test-time training with normalizing flow. In *2023 IEEE/CVF Winter Conference on Applications of Computer Vision (WACV)*, pages 2125–2126, Los Alamitos, CA, USA, Jan 2023. IEEE Computer Society. doi: 10.1109/WACV56688.2023.00216. URL <https://doi.ieeecomputersociety.org/10.1109/WACV56688.2023.00216>.
- Yossi Gandelsman, Yu Sun, Xinlei Chen, and Alexei A Efros. Test-time training with masked autoencoders. In Alice H. Oh, Alekh Agarwal, Danielle Belgrave, and Kyunghyun Cho, editors, *Advances in Neural Information Processing Systems*, 2022. URL <https://openreview.net/forum?id=SHM1lb7sjXk>.
- Gustavo A Vargas Hakim, David Osowiechi, Mehrdad Noori, Milad Cheraghalikhani, Ali Bahri, Ismail Ben Ayed, and Christian Desrosiers. Clust3: Information invariant test-time training. In *Proceedings of the IEEE/CVF International Conference on Computer Vision*, pages 6136–6145, 2023.
- David Osowiechi, Gustavo A. Vargas Hakim, Mehrdad Noori, Milad Cheraghalikhani, Ali Bahri, Moslem Yazdanpanah, Ismail Ben Ayed, and Christian Desrosiers. NC-TTT: A Noise Contrastive Approach for Test-Time Training, April 2024. URL <http://arxiv.org/abs/2404.08392>. arXiv:2404.08392 [cs].
- Glenn Shafer and Vladimir Vovk. A tutorial on conformal prediction. *Journal of Machine Learning Research*, 9(3), 2008.
- Anastasios N Angelopoulos and Stephen Bates. A gentle introduction to conformal prediction and distribution-free uncertainty quantification. *arXiv preprint arXiv:2107.07511*, 2021.
- Olivier Chapelle, Bernhard Scholkopf, and Alexander Zien. Semi-supervised learning. 2006. *Cambridge, Massachusetts: The MIT Press View Article*, 2, 2006.
- Ahmet Iscen, Giorgos Tolias, Yannis Avrithis, and Ondrej Chum. Label propagation for deep semi-supervised learning. In *Proceedings of the IEEE/CVF conference on computer vision and pattern recognition*, pages 5070–5079, 2019.
- Dan Hendrycks and Thomas Dietterich. Benchmarking neural network robustness to common corruptions and perturbations. 2019.
- Xingchao Peng, Ben Usman, Neela Kaushik, Dequan Wang, Judy Hoffman, and Kate Saenko. Visda: A synthetic-to-real benchmark for visual domain adaptation. In *Proceedings of the IEEE Conference on Computer Vision and Pattern Recognition (CVPR) Workshops*, June 2018.